Available online at www.sciencedirect.com
ScienceDirect
Journal of Solid State Chemistry 179 (2006) 4020–4028
JOURNAL OF SOLID STATE CHEMISTRY
www.elsevier.com/locate/jssc

Crystal structure of lanthanum bismuth silicate $Bi_{2-x}La_xSiO_5$ ($x\sim0.1$)

Samuel Georges*, François Goutenoire, Philippe Lacorre

Laboratoire des Oxydes et Fluorures UMR CNRS 6010, Université du Maine, Avenue Olivier Messiaen, 72085 Le Mans, France

Received 19 June 2006; received in revised form 29 August 2006; accepted 1 September 2006
Available online 22 September 2006

Abstract

A melting and glass recrystallization route was carried out to stabilize a new tetragonal form of Bi_2SiO_5 with bismuth partially substituted by lanthanum. The crystal structure of $Bi_{2-x}La_xSiO_5$ ($x\sim0.1$) was determined from powder X-ray and neutron diffraction data (space group $I4/mmm$, $a=b=3.8307(3)$ Å, $c=15.227(1)$ Å, $V=224.18$ Å^3, $Z=2$; reliability factors: $R_{Bragg}=5.65\%$, $R_p=14.6\%$, $R_{wp}=16.8\%$, $R_{exp}=8.3\%$, $\chi^2=8.3$ (X-ray) and $R_{Bragg}=2.40\%$, $R_p=8.1\%$, $R_{wp}=7.5\%$, $R_{exp}=4.2\%$, $\chi^2=3.3$ (neutrons); 11 structural parameters refined).

The main effect of lanthanum substitution is to introduce, by removing randomly some bismuth $6s^2$ lone pairs, a structural disorder in the surroundings of $(Bi_2O_2)^{2+}$ layers, that is in the $(SiO_3)^{2-}$ pyroxene files arrangement. It results in a symmetry increase relatively to the parent compound Bi_2SiO_5, which is orthorhombic. The two structures are compared.

Keywords: Bismuth lanthanum silicon oxide; Crystal structure; Powder X-ray and neutron diffraction; Crystallization from glass phase; Disordered pyroxene files

1. Introduction

The Aurivillius phases have been studied for a long time for interesting ferroelectric properties [1–3]. The general formula of this structural family is $[Bi_2O_2][A_mB_{m-1}O_{3m+1}]$. Their structure is built up from an intergrowth of $[Bi_2O_2]^{2+}$ layers and $[A_mB_{m-1}O_{3m+1}]^{2-}$ perovskite-type sheets [4–6]. The $[Bi_2O_2]^{2+}$ layers consist of oxygen-based square pyramids, the apex being occupied by Bi^{3+}. This geometry is attributed to the electronic configuration of Bi^{3+}: [Xe] $4f^{14}5d^{10}6s^2$, where the electronic $6s^2$ lone pair presents a high polarizability responsible for the stereochemical activity of the Bi^{3+} cation [7–10]. In the general formula $[Bi_2O_2][A_mB_{m-1}O_{3m+1}]$, m is the number of octahedra stacked along the direction perpendicular to the sheets. A and B are the 6-fold and 12-fold (perovskite cage) coordination sites of the perovskite layers respectively.

When $m=1$, the perovskite layer is a single RO_4 type slab, as observed in Bi_2WO_6 ($[Bi_2O_2]^{2+}$, $[WO_4]^{2-}$). For cations with lower oxidation states, the perovskite layers become deficient and reduced to pyroxene files layers, as observed in Bi_2GeO_5 ($[Bi_2O_2]^{2+}$, $[GeO_3]^{2-}$).

Another Aurivillius phase, $Bi_4V_2O_{11}$, built up from an intergrowth of $(Bi_2O_2)^{2+}$ layers and deficient perovskite layers $(VO_{3.5}\square_{0.5})^{2-}$ [11], presents a high oxide-ion conductivity because of the oxygen vacancies in the deficient perovskite layers. $Bi_4V_2O_{11}$ is the parent compound of the BIMEVOX family, widely studied as oxide-ion conductors [12,13].

The orthorhombic Bi_2SiO_5 form was studied as insulator buffer layer for the deposition of $Bi_4Ti_3O_{12}$ thin films for ferroelectric systems [14–18]. Its two-dimensional structure [19] is built up from an intergrowth of $(SiO_3)^{2-}$ pyroxene files layers inserted between $(Bi_2O_2)^{2+}$ layers. The structure is represented in Fig. 1. The $(Bi_2O_2)^{2+}$ layers are formed of slightly distorted squared oxygen planes. These squares are capped alternatively above and below by the bismuth atoms. This configuration indicates the strong steric activity of the bismuth $6s^2$ lone pair. Given the coordination sphere of the bismuth atoms, the lone pair seems to point in the opposite relative to oxygen squares, as suggested in Fig. 1 by the black arrows. Pyroxene files layers are made of corner-sharing SiO_4 tetrahedra in

*Corresponding author. Fax: +33 0 4 768 26670.
E-mail address: samuel.georges@lepmi.inpg.fr (S. Georges).

0022-4596/$ - see front matter © 2006 Elsevier Inc. All rights reserved.
doi:10.1016/j.jssc.2006.09.011

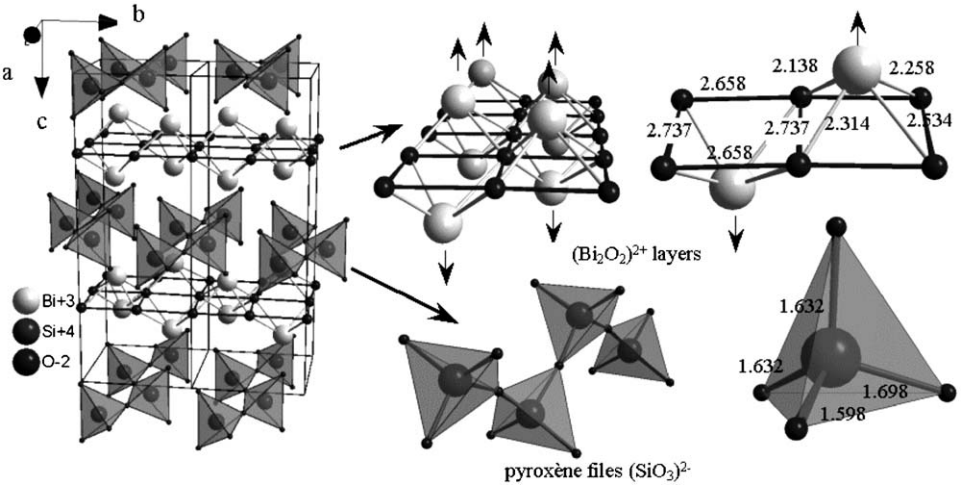

Fig. 1. Structural representation of orthorhombic Bi_2SiO_5 (from Ref. [19]).

columns parallel to $(Bi_2O_2)^{2+}$ planes. The SiO_4 tetrahedra are slightly distorted as illustrated in Fig. 1.

Here we present the synthesis, structure determination and analysis of a new tetragonal form of Bi_2SiO_5-type oxide obtained by partial substitution of Bi^{3+} by La^{3+}: $Bi_{2-x}La_xSiO_5$ ($x\sim0.1$).

2. Experimental

2.1. Synthesis

Two methods were used for the preparation of Bi_2SiO_5 and $Bi_{2-x}La_xSiO_5$ ($x\sim0.1$). The first one was a conventional solid-state reaction in air at 950 °C for 24 h between the starting oxides Bi_2O_3, La_2O_3 and SiO_2, previously ground together in ethanol in an agate mortar.

The second method had previously been reported for the synthesis of the bismuth silicate $Bi_4Si_3O_{12}$, among others [20,21]. The $Bi_{1.9}La_{0.1}SiO_5$ stoichiometric mixture of starting oxides was molten in air in a platinum boat at 1050 °C, and quenched in cold water, which led to an amorphous yellow glass. The latter was ground in an agate mortar and crystallized in air at 550 °C for 12 h. For both methods, lanthanum oxide La_2O_3 was heated in air at 1000 °C for one night and placed in a dessicator prior to weigh-in, in order to avoid hydratation and/or carbonatation.

2.2. Thermal analysis

In order to optimize the synthesis conditions for the melting method, Differential Thermal Analyses (DTA) have been carried out to determine the glass transition temperature T_g, the crystallization temperature of the compounds, and to detect their melting points. Differential thermal analyses were carried out in dried argon flow on a TA instruments SDT 2960. An amount of 40–50 mg of powder was exactly weighted, placed in a platinum crucible, and heated from room temperature to approximately 900 °C with a constant heating rate of 15 °C/min. The apparatus furnace was turned off just after melting (see after), to avoid deterioration.

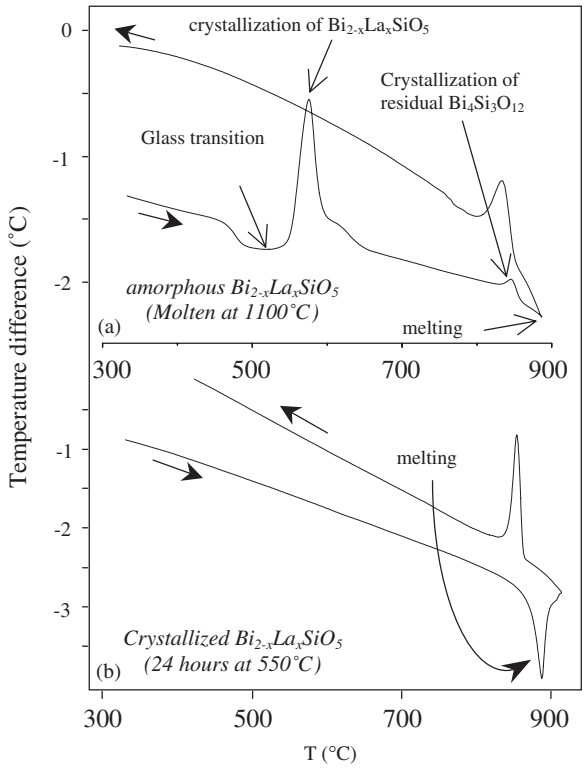

Fig. 2. Differential thermal analyses carried out in argon: (a) for a quenched and ground amorphous $Bi_{2-x}La_xSiO_5$ phase and (b) for a crystallized $Bi_{2-x}La_xSiO_5$ phase.

2.3. Structural characterization

The compounds synthesized by both methods (see experimental section) have been characterized by powder X-ray diffraction. The X-ray diffraction data were

collected on a SIEMENS D 5000 Bragg-Brentano diffractometer for routine collection (phases identification), and on a BRUKER AXS D8 Bragg-Brentano diffractometer for the long-collection patterns (structural refinements).

For the latter, a 2θ range of 10–100° was chosen, with 70 s counting time for each 0.04° step using the copper wavelength : λ (Cu$K\alpha$) = 1.5406 Å. The powders were spread with a 100 μm sieve in order to limit a preferred orientation phenomenon due to the anisotropy of the crystal structure.

Room temperature neutron diffraction pattern was collected on the Debye-Sherrer diffractometer D2B of Institut Laue-Langevin (ILL-Grenoble, France). The 2θ range was $-6°$ to $-160°$, the step 0.05°, and the total collecting time 2 h, with $\lambda = 1.59709$ Å. The sample of 40 g of powder was placed in a vanadium container.

3. Results

3.1. Thermal properties

The DTA curve presented in Fig. 2a was recorded on a powder prepared from the quenched and ground glass with a nominal composition $Bi_{1.9}La_{0.1}SiO_5$. This curve is characteristic of an amorphous state. The glass transition occurs at about 500 °C, and is followed by a strong exothermal signal at about 550 °C, indicating the crystallization of the Bi_2SiO_5 type phase (see next section for the corresponding structural data). The shape of this peak indicates a fast crystallization process. At higher temperatures, a small and wide exothermal peak appears, probably due to the crystallization of residual $Bi_4Si_3O_{12}$ (also detected by X-ray diffraction, see after). The latter is followed by the melting of the powder, at about 900 °C. The exothermal solidification signal is detected upon cooling. Part b of Fig. 2 presents a differential thermal analysis curve, obtained on the same compound after crystallization (quenched, ground and crystallized material). It does not present any thermal signal below 885 °C, indicating that no structural phase transition occurs in the crystallized compound before melting.

3.2. Phase characterization and symmetry

The powder diffraction pattern of the substituted compound (with nominal composition $Bi_{1.9}La_{0.1}SiO_5$) prepared by solid-state reaction is given in Fig. 3a. The powder is composed of a mixture of Bi_2O_3 and $Bi_4Si_3O_{12}$. Obviously, this method, with the applied conditions, is

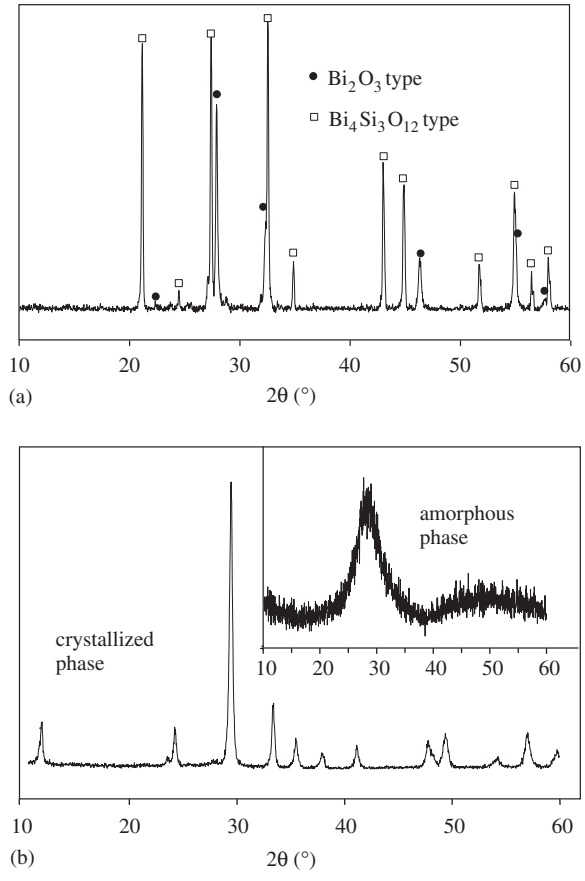

Fig. 3. Powder X-ray diffraction patterns of the products resulting from the two synthetic routes described in the text: (a) solid state reaction (mixture of phases) and (b) melting route ($Bi_{2-x}La_xSiO_5$).

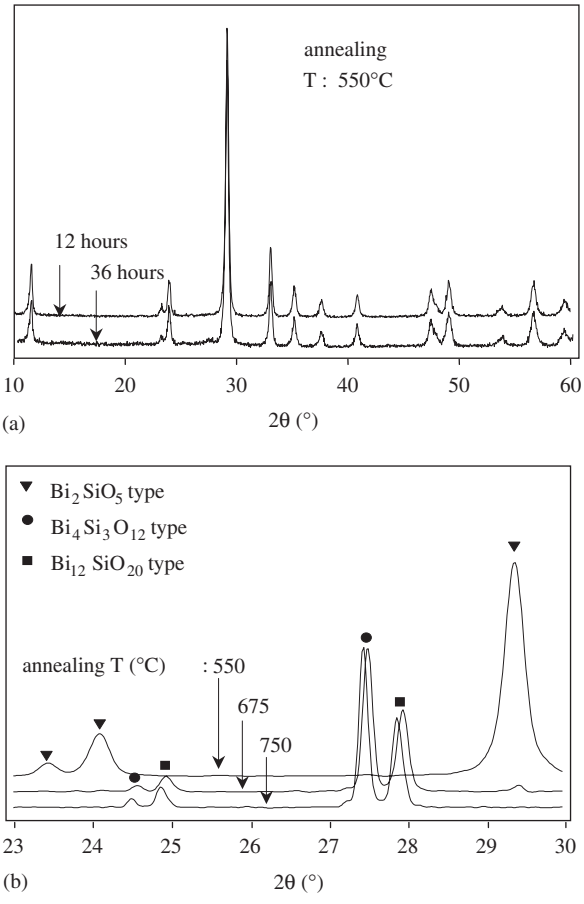

Fig. 4. Powder X-ray diffraction patterns of : (a) $Bi_{2-x}La_xSiO_5$ annealed at 550 °C for different times ; (b) $Bi_{2-x}La_xSiO_5$ annealed for 12 h at different temperatures.

unsatisfying for the preparation of the bismuth silicate Bi_2SiO_5 type phase. Powder X-ray diffraction patterns for the synthesis of $Bi_{2-x}La_xSiO_5$ ($x\sim0.1$) from the melt are given in Fig. 3b. The pattern of the glass (insert) is obtained after quenching from the melt, and the pattern of the crystallized phase after annealing of the ground glass at 550 °C. Both are in agreement with thermal analyses. The same behaviour was observed for Bi_2SiO_5. Both compounds were then prepared by the melting route.

The effects of both sintering time and temperature have been explored in order to optimize the synthesis conditions. Fig. 4a indicates that 12 h at 550 °C is enough to crystallize the amorphous $Bi_{2-x}La_xSiO_5$ type phase. Fig. 4b shows that for higher temperatures, crystallization of supplementary phases isostructural to $Bi_4Si_3O_{12}$ and $Bi_{12}SiO_{20}$ occurs, indicating the metastability of Bi_2SiO_5 type oxides. After several hours at 750 °C, the $Bi_{1.9}La_{0.1}SiO_5$ phase is completely decomposed.

Long collection diffraction patterns of Bi_2SiO_5 and $Bi_{1.9}La_{0.1}SiO_5$ are presented in Fig. 5. The broad diffraction peaks may be the consequence of the crystallization from a glass, which leads to very small crystallographic coherent domains. Bi_2SiO_5 pattern can be indexed in the orthorhombic space group $Cmc2_1$, with $a = 5.325(7)$ Å, $b = 5.477(1)$ Å, $c = 15.217(2)$ Å, $V = 221.95$ Å and $Z = 4$, in agreement with the previous report by Keller et al. [19]. The $Bi_{1.9}La_{0.1}SiO_5$ pattern looks slightly different, with the disappearance of some reflexions indicating a symmetry increase. In first approximation, this pattern can be indexed in a body-centered tetragonal space group, with $a\sim3.8$ Å, $c\sim15.2$ Å and $Z = 2$. The relationships between the orthorhombic and tetragonal cells, and between each set of cell parameters are given in Fig. 5 (inset).

The substituted phase obtained in this work presents a different structure than that of the parent compound.

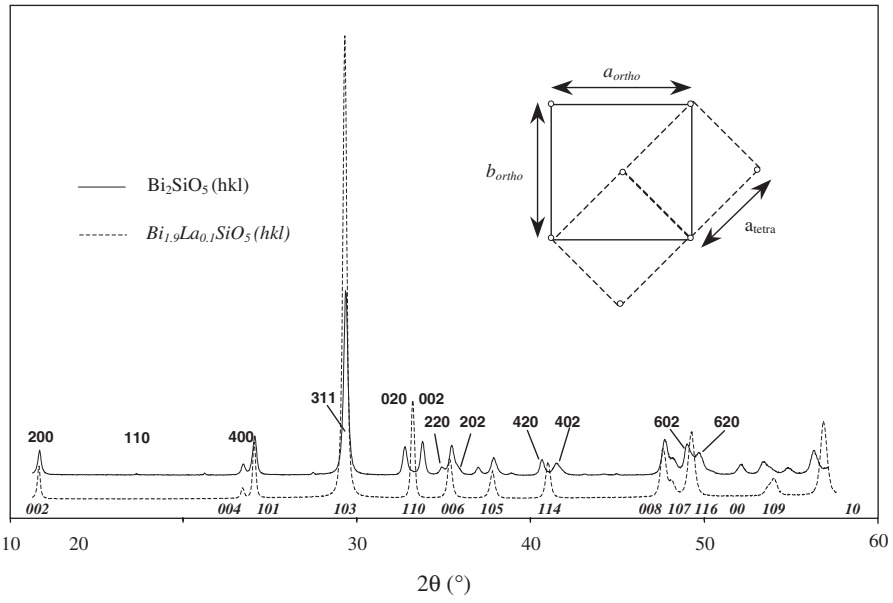

Fig. 5. Powder X-ray diffraction patterns of Bi_2SiO_5 (full line) and $Bi_{2-x}La_xSiO_5$ (dashed line) (in insert: orthorhombic and tetragonal cells relationships).

Table 1
Comparison between initial (A), intermediate (B,C) and final (D) structural models of $Bi_{2-x}La_xSiO_5$ ($x\sim0.1$), and respective fit reliabilities

Mod.	Atom	Position	x	y	z	Beq (Å^2)[a]	Occ.	R_{BRAGG} % (RX)	R_{BRAGG} %(neutrons)
A	Bi	4*e*	0	0	0.164(8)	1.946	3.80	6.01	5.32
	La	4*e*	0	0	0.164(8)	1.946	0.20		
	Si	2*b*	0	0	0.5	0.154	2.00		
	O1	4*d*	0	0.5	0.25	1.040	3.91		
	O2	4*c*	0.5	0	0	4.380	2.25		
	O3	4*e*	0	0	0.591(3)	3.256	3.90		
B	Si	8*h*	0.0701(5)		0.5	0.609	2.00	5.6	4.15
C	O3	16*m*	0.0665(3)		0.5917(6)	3.110	3.68	4.33	6.05
D[b]	Si	8*h*	0.0719(1)		0.5	0.120	2.00	5.65	2.4
	O3	16*m*	0.0697(4)		0.5913(2)	3.240	3.90		

[a]: $B_{eq} = 4/3a^2\,(\beta_{11} + \beta_{22} + \beta_{33})$.
[b]: SG : $I4/mmm$, $a = b = 3.8307(3)$ Å, $c = 15.227(1)$ Å, $V = 224.18$ Å^3, $Z = 2$; reliability factors: $R_{Bragg} = 5.65\%$, $R_p = 14.6\%$, $R_{wp} = 16.8\%$, $R_{exp} = 8.3\%$, $\chi^2 = 8.3$ (X-ray) and $R_{Bragg} = 2.40\%$, $R_p = 8.1\%$, $R_{wp} = 7.5\%$, $R_{exp} = 4.2\%$, $\chi^2 = 3.3$ (neutrons); number of structural parameters refined = 11.

Ketterer and Krämer [22] reported a Bi_2SiO_5 type phase with a tetragonal symmetry, whereas in this work, Bi_2SiO_5 is orthorhombic. We were unable to get any tetragonal phase of Bi_2SiO_5, suggesting that its stabilization might be due to the presence of some impurity in the starting materials. As a matter of fact, as pointed out in this work, a small doping on the Bi^{3+} site is likely to stabilize a higher symmetry phase.

3.3. Crystal structure of tetragonal $Bi_{1.9}La_{0.1}SiO_5$

The crystal structure determination of the tetragonal form was first carried out on the basis of the structural parameters of Bi_2CO_5 ($Bi_2O_2CO_3$) [24,25]. This compound crystallizes in a tetragonal cell, with a volume comparable to that of $Bi_{1.9}La_{0.1}SiO_5$ ($I4/mmm$, n° 135, $a = 3.865$ Å, $c = 13.675$ Å, $V = 204.28$ Å for $Z = 2$). Its structure is built up from the same $(Bi_2O_2)^{2+}$ layers, with the tetrahedra files replaced by isolated $(CO_3)^{2-}$ units. Given the tetrahedral surrounding of silicon atoms, four body centered tetragonal space groups were selected ($I4/mmm$, $I4_1$, $I4_1/a$ and $I-4$) from which $I4/mmm$ was selected given its centricity and the reflections existence conditions.

For the structure determination, the cationic positions and one oxygen position (O1 in 4*d* site) of Bi_2CO_5 were used.

We then tried to localize the missing oxygen positions by Fourier analyses of the X-ray diffraction pattern, unsuccessfully. A neutron diffraction pattern was then collected (see experimental section). By combining X-ray and neutron data, we performed series of Fourier analyses and structural refinements by the Rietveld method, using alternatively Gfou [26] and Fullprof [27] programs in order to localize and refine the atomic positions of the two missing oxygen sites. The Fourier difference maps allowed us to localize, from the observed intensities as extracted by program Fullprof, two oxygen positions in 4*c* and 4*e* sites of the $I4/mmm$ space group. Final structural models were obtained by combined refinement from X-ray and neutrons data (relative weight of 0.5 for each set of data) using program Fullprof. A first model, hereafter called model A, is presented in Table 1. In spite of a good reliability, for both X-ray and neutron data, the model did not take into account the small reflexion ((1 0 11), $2\theta \sim 75.42°$, $d_{10\ 11} \sim 1.3055$ Å) in the neutron diffraction pattern (see Fig. 6a for a detail of the neutron diffraction pattern, in the $[73° \leqslant 2\theta \leqslant 79°]$ range). Moreover, considering the tetrahedral coordination sphere for silicon atoms, it was difficult to build such an environment in model A, in which Si atoms are located on the 4-fold axis. Accordingly, several models were proposed to solve these problems. By moving either Si (model B) or O3 (model C, see Fig. 6) atoms from their initial special positions on the 4-fold axis (model A), the (1 0 11) reflexion still not appeared in the calculated diagram (Fig. 6b and 6c for models B and C respectively),

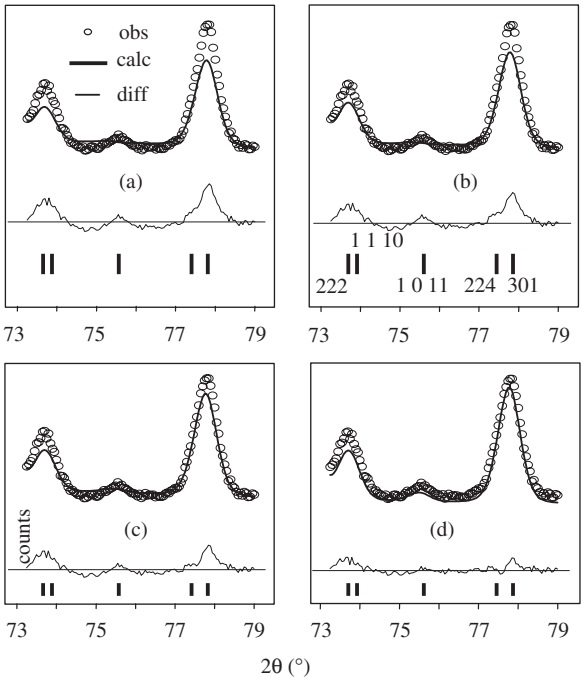

Fig. 6. Detail of the $[73° \leqslant 2\theta \leqslant -78.5°]$ range of the neutron diffraction pattern of $Bi_{2-x}La_xSiO_5$ including the (1 0 11) reflection, for models A(a), B(b), C(c) and D(d); see text for details.

Table 2
Final structural model of $Bi_{2-x}La_xSiO_5$ ($x \sim 0.1$) determined by coupled X-ray/neutrons data refinement

Atom	Position	*x*	*y*	*z*	Beq (Å^2)[a]	Occ.
Bi	4e	0	0	0.164(8)	1.946	3.8
La	4e	0	0	0.164(8)	1.946	0.2
Si	8 h	0.0719(1)	0.0719(1)	0.5	0.12	2.0
O1	4d	0	0.5	0.25	1.04	3.91
O2	4c	0.5	0	0	4.38	2.25
O3	16 m	0.0697(4)	0	0.5913(2)	3.24	3.90

Table 3
Refinement parameters for neutrons and X-ray patterns

	Neutrons	X-ray
λ (Å)	1.59709	1.54056 ($K\alpha_1$) 1.54433 ($K\alpha_2$)
Contribution	0.5	0.5
Calculated reflexions	88	51 (Kα1)
2θ range (°)	7 to 150	9 to 99
Step size	0.05	0.04
Profile function[a]	Pseudo-Voigt	Pseudo-Voigt
η	0.3846	0.5026
U	0.6435	1.9017
V	−0.3253	−1.1713
W	0.2627	0.3090
P1 [b]	0.0588	0.1166
P2 [b]	0.0182	0.0005

** Asymmetry correction [35]: $A = 1 + \{P1 \times Fa(z) + P2 \times Fb(z)\} \times \tan\theta$; with $z = (2\theta_i - 2\theta_{shift})/\mathrm{FWHM}$; $Fa(z) = 2z \times \exp(-z^2)$; $Fb(z) = 2(2z^2 - 3) \times Fa(z)$; $\mathrm{FWHM} = (U + V \tan\theta + W \tan^2\theta)^{1/2}$.

[a]Pseudo-voigt = (1−η) Gaussian + ηLorentzian.

whereas the reliability increased (Table 1). Thus, silicon atoms were splitted from the 2*b* site to an 8*h* site, and O3 atoms from the 4*e* site to a 16*m* site, with, as a consequence, a partial occupation of these positions (about $\frac{1}{4}$). Finally, the reliability factors were significantly much lower in the case of model D (Fig. 6d) in which both Si and O3 atoms are shifted from the 4-fold axis ($R_{Bragg} = 6.01\%$ (X-ray) and 5.32% (neutrons) for model A, and $R_{Bragg} = 5.65\%$ (X-ray) and 2.40% (neutrons) for model D), and for which the (1 0 11) reflexion appeared in the calculated diagram (see Fig. 6d).

The refined structural parameters and occupancies are presented in Table 1 for the three models, and the final structural model is given in Table 2 (see also in Table 3 the refinement parameters for both neutron and X-ray patterns).

The final refined patterns are presented in Fig. 7a for X-ray, and 7*b* for neutrons (note the presence of a small

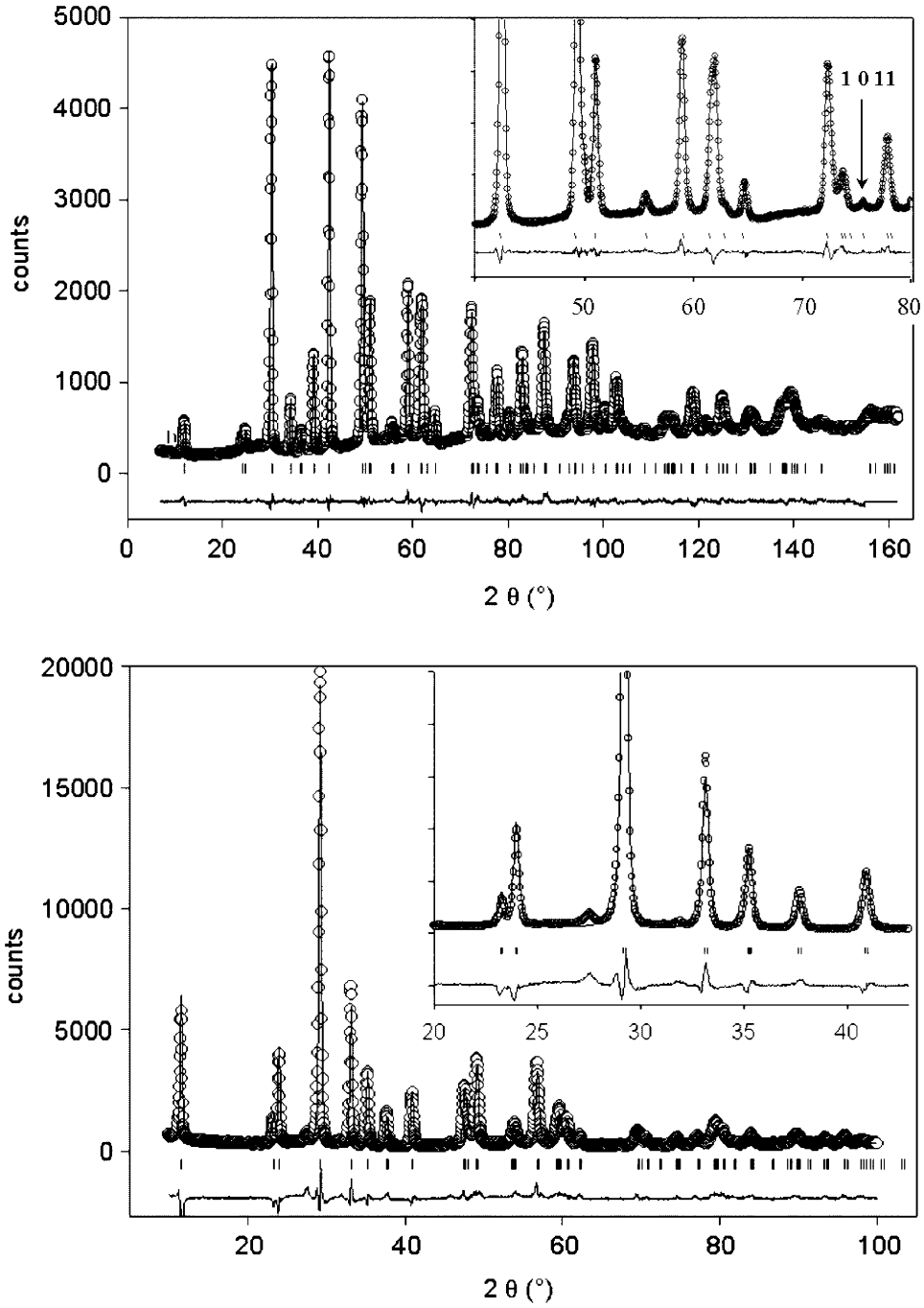

Fig. 7. Final refinement result for $Bi_{2-x}La_xSiO_5$. Observed (circles), calculated (line) and difference (below) patterns are presented for: lower) X-ray ($R_{Bragg} = 5.65\%$, $R_p = 14.6\%$, $R_{wp} = 16.8\%$, $R_{exp} = 8.3\%$, $\chi^2 = 8.3$); upper) Neutrons ($R_{Bragg} = 2.40\%$, $R_p = 8.1\%$, $R_{wp} = 7.5\%$, $R_{exp} = 4.2\%$, $\chi^2 = 3.3$).

unidentified impurity peak close to $2\theta = 28^\circ$ for the X-ray pattern). The refined cell parameters are $a = 3.8307(3)$ Å, $c = 15.227(1)$ Å and $V = 224.18$ Å^3 for $Z = 2$. We note that the average *ab* plane cell parameter in the orthorhombic form (according to Keller et al., [19]: $(2^{1/2}/4) \times (a + b) = 3.819$ Å, is very close to the $a = 3.8307(3)$ Å determined in the tetragonal cell for $Bi_{1.9}La_{0.1}SiO_5$ (this work). Interestingly, a slight cell volume increase (224.18 Å^3 against 221.95 Å^3 for $Z = 2$) was observed with the substitution in spite of the respective ionic radii of Bi^{3+} and La^{3+} in a 8-fold coordination sphere (according to Shannon and Prewitt [23, 28–30]: $r(Bi^{3+})_8 = 1.31$ Å; $r(La^{3+})_8 = 1.30$ Å).

4. Structure analysis and discussion

A representation of the final structural model is given in Fig. 8 with both Si and O3 splitted positions. The squared oxygen planes and the $(Bi_2O_2)^{2+}$ layers are ordered. On both sides, the (Bi/La) atoms are covered by 16 O3 atoms in statistical occupation (about $\frac{1}{4}$), and 4 O1 atoms. The mean coordination of (Bi/La) atoms is then close to 8. Given the splitting of Si and O3 sites, the (SiO_4) tetrahedra are disordered. Taking into account all the O3 positions, four tetrahedra SiO_4: ($Si(O2)_2(O3)_2$) are imbricated in each others. These entities could also be described as disordered anion deficient ($SiO_4\square_2$) octahedra (see Fig. 8b), with O2 and O3 occupying the equatorial and apical positions, respectively. This representation allows the visualization of the disorder introduced by the cationic substitution. The latter affects the $(SiO_3)^{2-}$ layers, whereas the substitution concerns the $(Bi_2O_2)^{2+}$ layers. This observation suggests that the disorder is created rather by the bismuth lone pair suppression than by the cationic substitution itself, which, again, gives a significant importance to the steric effect of these lone pairs in the atomic organization of such structures. In other words, the long-range order observed in the orthorhombic form may be partially due to the stereochemical activity of the lone pairs. The formal vacancies created by the lone pairs suppression, as suggested by Lacorre [31] (substitution of Bi^{3+} with lone pair by La^{3+} with comparable size but without lone pair), are randomly distributed between the two different layers, and are most likely responsible for the disorder observed in the tetragonal form.

The silicon environment is shown in Fig. 9. This coordination sphere was determined by selection of the

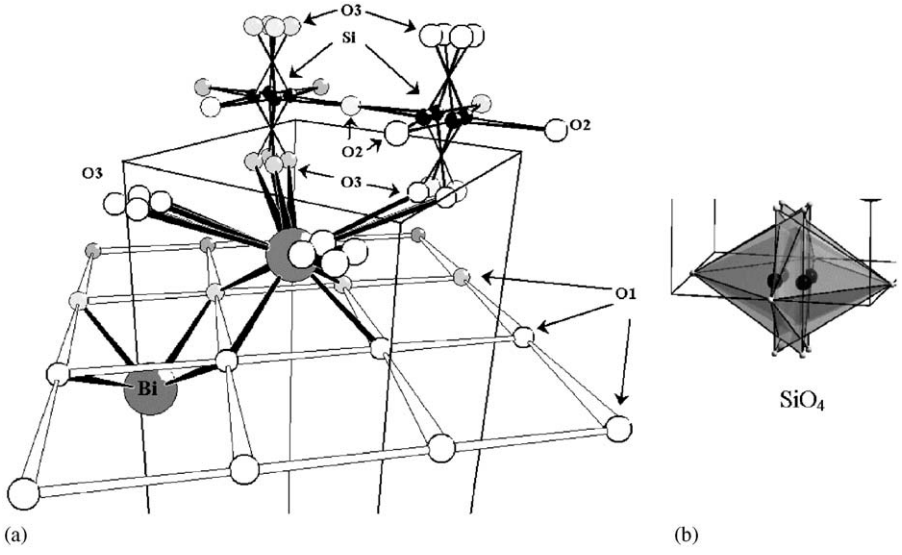

Fig. 8. (a) Final structural model of $Bi_{2-x}La_xSiO_5$, with split Si and O3 positions; (b) detail of the Si coordination sphere.

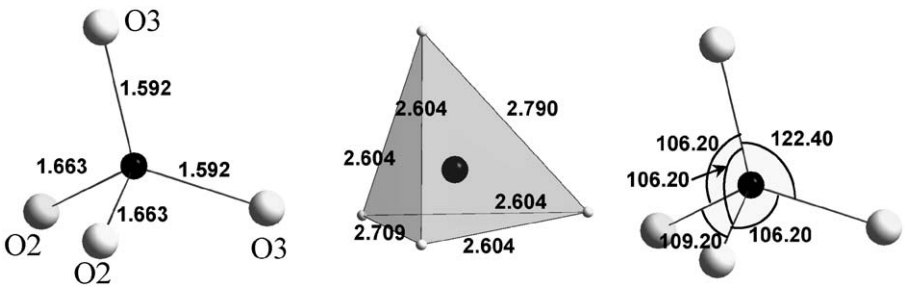

Fig. 9. Detail of a silicon coordination tetrahedron as extracted from the atomic distribution in random pyroxene files of tetragonal $Bi_{2-x}La_xSiO_5$; (distances : ±0.0005 Å; angles : ±0.05°).

most reasonable distances for Si–O bounds. Calculated distances and angles are characteristic of a SiO_4 tetrahedra. The Si–O2 and Si–O3 distances (see Fig. 9) are, respectively, 1.663(1) and 1.592(1) Å. The Si valence computed from these distances using the O'Keeffe and Brese bond-valence parameters [32] is very close to the expected 4 (3.98 for full site occupancies). The O3–Si–O3 angle is more obtuse in the tetragonal form than in the orthorhombic one (122.39(1)° and 117.63(1)°, respectively).

A local ordered description of the final $Bi_{1.9}La_{0.1}SiO_5$ structure is proposed in Fig. 10, and compared to the Bi_2SiO_5 orthorhombic structure. This description takes into account the stoichiometry of the $Bi_{1.9}La_{0.1}SiO_5$ phase. It has been built by selecting the most probable SiO_4 units, and considering a mean occupation factor for the global Si and O3 sites of $\frac{1}{4}$. In this representation, the pyroxene files orientations alternate along $(a+b)$ and along $(a-b)$, as a direct consequence of the substitution and of the disorder.

Instead of being all ordered along the a-axis in Bi_2SiO_5, the tetrahedra files are randomly orientated along $(a+b)$ or $(a-b)$ in the tetragonal $Bi_{1.9}La_{0.1}SiO_5$ phase, creating random A and/or B sequences in the ab plane (see Fig. 10b). The construction of this ordered representation

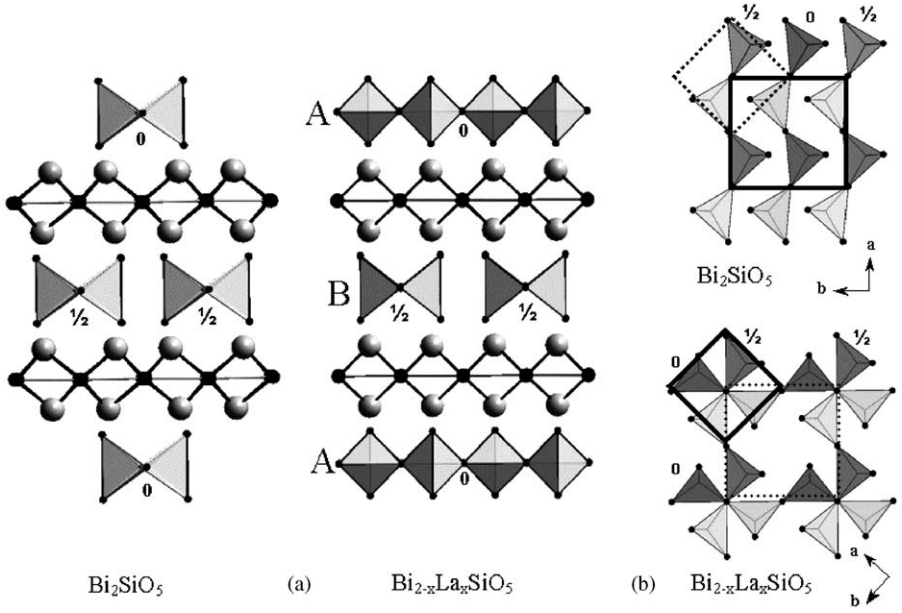

Fig. 10. Structural relationships between Bi_2SiO_5 and $Bi_{2-x}La_xSiO_5$: (a) Projection along the a-axis for Bi_2SiO_5, and along the [110] axis for the local ordered description of $Bi_{2-x}La_xSiO_5$; (b) Projection along the c-axis.

Table 4
Selected inter-atomic distances and angles of Bi_2SiO_5 [19] and $Bi_{2-x}La_xSiO_5$ (x∼0.1) [this work]

	Distances (Å)									
	Bi–O1	Bi–O3	Bi–Bi	Si–O2	Si–O3	Si–Si	O1–O1	O2–O3	O2–O2	O3–O3
BS[a]	2.138(1) 2.258(1) 2.534(1) 2.314(1)	2.593(1) 3.189(1)	3.566(1) 3.724(1) 4.077(1)	1.598(1) 1.698(1)	1.632(1)	3.275(1)	2.658(1) 2.737(1)	2.626(1) 2.670(1)	2.667(1)	2.792(1)
BLS[b]	2.316(1)	2.956(1)	3.759(1) 3.831(1)	1.663(1)	1.592(1)	3.326(1)	2.709(1)	2.604(1)	2.709(1)	2.790(1)
	Angles (°)									
	Bi–Bi–Bi	Si–Si–Si	O3–Si–O3	O3–Si–O2	O2–Si–O2	O1–O1–O1	O2–O2–O2	O1–Bi–O1		
BS[a]	96.29(1) 81.31(1)	108.41(1)	117.63(1)	108.79(1) 106.61(1)	108.02(1)	87.88(1) 92.12(1)	169.64(1)	74.36(1) 75.74(1) 66.31(1) 69.37(1)		
BLS[b]	90.00	109.03(1)	122.39(1)	106.24(1)	109.03(1)	90.00	180.00	71.58(1)		

[a]: Bi_2SiO_5.
[b]: $Bi_{1.9}La_{0.1}SiO_5$.

allowed the calculation of the main interatomic (mean) distances and angles, for comparison with those of orthorhombic Bi_2SiO_5. These values are reported in Table 4. In most cases, the calculated values for the tetragonal form lie in the range of those observed for the corresponding lower symmetry orthorhombic phase.

Finally, note that a recent study from Grice et al. [33,34], proposed a solution to the crystal structures of kettnerite, bismutite $Bi_2(CO_3)O_2$, and beyerite $CaBi_2(CO_3)_2O_2$, structures close to that of substituted Bi_2SiO_5 presented in this work. Using single crystal diffraction data, the authors introduced a twin plane via reflection on {110} in an orthorhombic symmetry (*Immm*, $Z = 2$). The latter simulates tetragonal diffraction-intensity distribution for the pseudo-merohedral twin, and gives a structure with a correct stereochemistry, whereas the use of the tetragonal symmetry led to stereochemical incompatibilities relative to the placement of the $(CO_3)^{2-}$ groups.

Such a twin plane may also account for the structure of $Bi_{1.9}La_{0.1}SiO_5$, as the disordered model proposed in the current study. Further work will be required to clarify this point.

5. Conclusion

A tetragonal form of Bi_2SiO_5 was stabilized by partial substitution of Bi^{3+} by La^{3+} after recrystallization of a glass form with the same composition. The Bi^{3+} lone-pair disordering due to the substitution is most probably responsible for the observed disordering of pyroxene files layers in between the ordered $[Bi_2O_2]^{2+}$ layers, as compared to the fully ordered orthorhombic structure of Bi_2SiO_5.

Acknowledgment

The authors express their thanks to E. Suard (Institut Laue-Langevin, Grenoble, France) for neutron diffraction pattern collection, and ADEME and Rhodia for financial support.

References

[1] B. Aurivillius, P.H. Fang, Phys. Rev. 126 (1962) 893–896.
[2] E.C. Subbarao, Phys. Rev. 122 (1961) 804–807.
[3] P.H. Fang, C.R. Robbins, B. Aurivillius, Phys. Rev. 126 (1962) 892.
[4] B. Aurivillius, Ark. Kemi 2 (1950) 519.
[5] J.L. Hutchinson, J.S. Anderson, C.N.R. Rao, Proc. R. Soc. London Ser. A 355 (1977) 301.
[6] B. Frit, J.P. Mercurio, J. Alloys Cd. 188 (1992) 27.
[7] R.G. Gillespie, R.G. Nyholm, Quart. Rev. Chem. Soc. 11 (1957) 339.
[8] I.D. Brown, J. Solid State Chem. 11 (1974) 214.
[9] J. Galy, G. Meunier, S. Andersson, A. Aström, J. Solid State Chem. 13 (1975) 142.
[10] G. Bergerhoff, Acta Cryst. 15 (1962) 509.
[11] F. Abraham, J.C. Boivin, G. Mairesse, G. Nowogrocki, Solid State Ionics 40–41 (1990) 934.
[12] T. Iharada, A. Hammou, J. Fouletier, M. Kleitz, J.C. Boivin, G. Mairesse, Solid State Ionics 48 (1991) 257.
[13] S. Lazure, C. Vernochet, R.N. Vannier, G. Nowogrocki, G. Mairesse, Solid State Ionics 90 (1-4) (1996) 117–123.
[14] T. Kijima, H. Matsunaga, Jpn. J. Appl. Phys. I 37 (1998) 5171–5173.
[15] T. Kijima, Integrat. Ferroelectric 26 (1999) 795–803.
[16] T. Kijima, H. Matsunaga, Jpn. J. Appl. Phys. I 38 (1999) 2281–2284.
[17] T. Kijima, Electron. Commun. Jpn. II—Electronics 84 (2001) 49–58.
[18] J. Harjuoja, S. Vayrynen, M. Putkonen, L. Niinisto, E. Rauhala E, J. Cryst. Growth 286 (2006) 376–383.
[19] Keller et al., ICDD 36-0287 and 36-0288 files.
[20] P. Beneventi, D. Bersani, P.P. Lottici, Solid State Commun. 93 (2) (1995) 143–146.
[21] M. Ishii, K. Harada, N. Senguttuvan, M. Kobayashi, I. Yamaga, J. Cryst. Growth 205 (1999) 191–195.
[22] J. Ketterer, V. Krämer, N. Jb. Miner. Mh. 1 (1986) 13–18.
[23] D.R. Lide, Handbook of Chemistry and Physics, 79th ed.
[24] A. Lagergantz, L.A. Sillén, Arkiv. Kemi, Mineral Geol. A 25 (1948) 1–21.
[25] C. Greaves, S. Blower, Mater. Res. Bull. 23 (1988) 1001–1008.
[26] J. Gonzalez-Platas, J. Rodriguez-Carvajal, Graphic Fourier Program (Gfou) Vol. 1.12, Laboratoire Léon Brillouin CEA-CNRS, Centre d'Etudes de Saclay, France.
[27] J. Rodriguez-Carvajal, Program Fullprof.2k, version 2.00, 2001.
[28] R.D. Shannon, C.T. Prewitt, Acta. Cryst. B 25 (1969) 925.
[29] R.D. Shannon, C.T. Prewitt, Acta. Cryst. B 26 (1970) 1046.
[30] R.D. Shannon, Acta. Cryst. A 32 (1976) 751.
[31] P. Lacorre, Solid State Sci. 2 (2000) 755–758.
[32] N.E. Brese, M. O'Keeffe, Acta Cryst. B 48 (1991) 192.
[33] J.D. Grice, M.A. Cooper, F.C. Hawthorne, Can. Mineral. 37 (1999) 923–927.
[34] J.D. Grice, Can. Mineral. 40 (2002) 693–698.
[35] J.F. Berar, G. Baldinozzi, J. Appl. Cryst. 26 (1993) 128.